Summer 2022

Exploration of Novel Nickel Metal Organic Decomposition Inks

Ivy Tran
San Jose State University

EXPLORATION OF NOVEL NICKEL METAL ORGANIC DECOMPOSITION INKS

A Project

Presented to

The Faculty of the Department of Chemistry

San José State University

In Partial Fulfillment

of the Requirements for the Degree

Master of Science

by

Ivy Tran

August 2022

The Designated Project Committee Approves the Project Titled

EXPLORATION OF NOVEL NICKEL METAL ORGANIC DECOMPOSITION INKS

by

Ivy Tran

APPROVED FOR THE CHEMISTRY DEPARTMENT

SAN JOSÉ STATE UNIVERSITY

August 2022

Roger Terrill, Ph.D.	Chemistry Department
Madalyn Radlauer, Ph.D.	Chemistry Department
Philip Dirlam, Ph.D.	Chemistry Department

ABSTRACT

EXPLORATION OF NOVEL NICKEL METAL ORGANIC DECOMPOSITION INKS

By Ivy Tran

In the growing and ever-evolving world of technology, the prospect of printable and flexible electronics has become prominent. Printable metal inks are of significant interest as they can be used to fabricate metal films efficiently, with greener materials, at lower-cost, and with low-waste as compared to conventional metal film deposition techniques. They also allow the utilization of a wider range of materials, giving way to flexible technologies in the future. Here, we introduce the formulation of novel nickel-precursor based liquid organometallic decomposing (MOD) inks that sinter at relatively low temperatures and thermally decompose into a conductive layer. In this work, nickel metal carboxylate salts were combined with liquid amino-alcohols to form these novel inks. These materials decompose at temperatures around 300 °C, leaving behind reduced metal and other gas-phase products. Our intent is to produce uniform metal mirrors with high conductivity and very low waste. To achieve this we prepared novel nickel MOD inks and characterized the inks, the decomposition process, and the prepared metal films that they produce.

ACKNOWLEDGEMENTS

I owe great gratitude and appreciation for Dr. Terrill's mentorship and support throughout my thesis project and graduate studies. His willingness and desire to foster student success is more than apparent, not only in the research group but beyond. I would also like to that Dr. Sunity Sharma for his incredible knowledge of chemistry and MOD inks. It was amazing to work with someone with such an eagerness and passion for chemistry. Thank you to Dr. Madalyn Radlauer and Dr. Philip Dirlam for their patience and feedback throughout each part of my thesis as my thesis committee. An honorable mention goes to Dr. Abraham Wolcott, who made it possible for us to use the thermogravimetric analysis (TGA) instrument, which has been crucial to this thesis, and who has provided much moral support. I would also like to give a nod to my lab mates and peers, who shared in many of the same struggles and celebrated in many successes. Special thanks to my friends and family, as well as the greater community of San Jose State University and the thesis reviewers.

TABLE OF CONTENTS

LIST OF TABLES

LIST OF FIGURES

1. INTRODUCTION

Conventional metal film deposition techniques,[1] including vapor-deposition, sputter-deposition, and electroplating, are complicated and often require strict operating and environmental conditions. Some strict conditions include needing vacuum environments and high temperatures. They can also be fairly expensive and wasteful.[2, 3]

Inkjet printing, which is a direct additive deposition process, is a new trend in the development of electronic products.[2, 4-6] This format yields low-cost, low-waste, comparatively fast, and non-contact processing of printed circuits. They also have the unique capability for the use of flexible substrates such as paper, fabric, and plastics, due to the low temperatures achievable for fabrication.[2, 3, 5, 7]

Printable flexible technology can be used in a wide range of fields and applications. In the electronics sector, printing can be used for flexible circuit boards, displays and sensors.[2, 8] In energy technology, it can be useful for battery materials[9] and as a catalyst[10-12] e.g., for water electrolysis. In medicine or biology, there is potential for use in biotech fabrication, such as for ECG, EEG, and other sensor-based monitors.[6] Printing technology can also give rise to items such as wearable electronics, thinner and lighter technology, and even improvement of foldable technology like phones and tablets.[3]

1.1 Project Intent and Summary

In this Thesis, the intent is to fabricate conductive ink from nickel. Specifically, we want inks that sinter at low temperatures but yield conductive metallic films. Our approach is to explore the chemistry of self-reduction, as demonstrated by the reaction below:

$$\mathbf{Ni(COOR)_2 \rightarrow Ni + 2\ CO_2 + gasses} \quad (1)$$

The resulting inks should be stable, the product will be a reduced metal, and the surface of the metallic films should be free of oxides.

In summary, this Thesis will describe the preparation and characterization of novel nickel metal organic decomposition (MOD) ink materials and their metal film products.

1.2 Metal Organic Decomposition (MOD) Inks

A MOD ink is a stable solution which can be coated onto a surface and then heated to be transformed into pure metal.[7, 8] The general decomposition mechanism that occurs us a reduction such as Reaction (1), above. They are homogeneous, particle-free metal solutions,[3, 13] unlike the relatively prevalent metal nanoparticle-based (NP) inks.

The successful metal NP ink requires good control over preparation processes and can suffer from particle agglomeration[14] and oxidation issues.[15] NP inks also often require higher sintering temperatures relative to MOD equivalents.[15]

MOD inks, in comparison, are simple to prepare as they are simply cationic metals coordinated to ligands and dissolved in suitable solvents. Preparation of a MOD ink can be as simple as dissolving a metal precursor in a volatile solvent, as the metal film formation process may also be as simple as heating to volatilize the solvent and reduce the metals.

At its most basic, MOD inks are composed simply of a metal-organic compound (usually a metal salt) and a volatile solvent (usually organic), with potential additives.[16-18] When sintered and reduced, they leave behind a pure metal film only where they are coated, with

little to no waste produced. They experience relatively low-temperature decomposition processes, though little is known about the details and mechanism of the self-reduction chemistry of MOD inks in general. This work focuses on metal carboxylate-amine complexes dissolved in organic solvents, particularly.

1.3 Selection of Materials

Various organometallic compounds, amines, and solvents lead to successful MOD compositions, i.e. those with stable precursor inks that produce clean metallic films. Two organometallic compounds (nickel (II) acetate and nickel (II) butyrate) and two amine-solvents were compared in this work.

1.3.1 Selection of Nickel

It is imperative that great care is taken when selecting an organometallic compound that will be the basis of the MOD ink materials of study. The organometallic compound will influence not only the thermal, electrical, and conductive properties of the final metal films, they will also influence the thermal decomposition and reduction temperatures needed in film formation. To achieve relatively-low sintering temperatures, a metal-carboxylate is selected for their low-temperature decarboxylation reactions.[19, 20]

Though there is some published work on nickel NP inks,[2, 12, 21-23] there is little existing published work on particle-free nickel inks,[2, 7] such as the ones studied in this work. DeBruin[7] describes a set of three particle-free and low temperature MOD reactive inks able to react to generate reduced Ni^0 metal on plastic and paper substrates at temperatures <100 °C. These inks used nickel acetate and three various solvent combinations:

1) ammonia, water, glycerol, 2) NaOH and propylene glycol, and 3) TMAH and propylene glycol. One of the earliest particle-free nickel inks was reported in 2007 by Pasquarelli,[24] who developed a nickel reactive ink used on glass and ZnO substrates at around 140-180 °C. This ink contained a nickel precursor, organic solvent, and organic additives. If the ink is good, then the only reason that we are using the butyrate/amine approach is to make an ink compatible with the Cu/Ag/Au/Pd compatible (i.e. for mixing to generate alloy films) ones that we have been developing in the Terrill lab. Ingredients including TMAH (a strong Arrhenius base) and glycerol (a reducing alcohol) are incompatible with the metal carboxylate inks that we have developed.

Li et al.[25] was able to develop a self-reducing nickel reactive ink that could be used in inkjet printing applications. This ink was created from aqueous nickel sulfate and sodium borohydride, which were printed in consecutive streams in an inkjet printer instead of mixed as a single solvent. This, however, left large salt deposit contamination after print. Petukhov et al.[26] took a similar inkjet printing approach but combined this with electroless plating (a.k.a. chemical plating) for metallization. After printing with nickel sulfate and sodium borohydride, the substrate was placed into an electroless plating bath with nickel sulfate and sodium hypophosphite to complete metallization of the bulk coating, yielding a Ni-P film.

Ginley et al.[27] was able to obtain a patent for a nickel formate, ethylene glycol, and ethylene diamine self-reducing nickel ink that sintered at 250 °C to yield a pure metallic film via spray printing onto glass substrates in open atmosphere. Other nickel reactive particle-free inks contain or yield nickel alloys or nickel alloy films.

Gold,[28] silver,[14, 29] and copper[13] are the most commonly-employed metals for the development of MOD and NP (colloidal) inks. This is due to the facile reduction of the Au, Ag, and Cu cations, the relative immunity of the reduced metal to reaction with oxygen, and their excellent properties as reduced metal contacts.

Nickel is known to have excellent conductivity and mechanical properties and has been known to be a good catalyst for H_2 production in water electrolysis. The element also has high corrosion resistance and has been seen to have interesting film chemistry.[30] Nickel, in comparison to metals like Cu, Ag, and Au that have been extensively explored in MOD ink materials, is also relatively inexpensive and plentiful.[22] These properties, combined with the fact that there is very little existing published work at the time of this writing,[7] were heavy driving factors in the selection of nickel as the focus of this project.

Nickel (II) acetate was initially chosen as the first metal-carboxylate compound due to its simplicity and wide availability.[12] Nickel (II) butyrate was synthesized from the nickel (II) acetate for variety in MOD ink preparation and exploration.

1.3.2 Selection of Ligand-Solvents

The solvents used in MOD ink preparation should also be ligand precursors that promote reduction[16] and are easily evaporated. They should also ideally be compatible for use in commercial printing, such as inkjet, which is the ultimate goal of the research project. The organometallic compounds should easily and fully dissolve in these solvents. The solvent should also leave no residue upon volatilization during the thermal decomposition process. Amines[16, 31, 32] are able to capture many of these properties and are also able to lower the

decomposition temperature of the metal precursors, making them highly desirable solvents to select for this project.

Pyridine, cyclohexylamine, methacrylic acid, 1-butanol, dimethylethanolamine, and ethanolamine used to prepare MOD inks, as detailed in a later section.

2. MATERIALS AND METHODS

2.1 Materials

Below in Table 1 is a table of reagents used in ink synthesis.

Table 1. Table of Materials

Material	**Supplier**	**Purity**
Nickel (II) Acetate Tetrahydrate	Alfa Aesar	98+%
Acetic Acid	Aldrich	99%
Acetic Anhydride	Aldrich	99%
Butyric Acid	Alfa Aesar	99+%
1-butanol	Alfa Aesar	99%
Ethanolamine	Alfa Aesar	98+%
Dimethylethanolamine	Acros Organics	99%
Pyridine	Fisher Chemical	98+%
Cyclohexylamine	Alfa Aesar	99%
Methacrylic acid	Acros Organics	99.5%
Nitrogen gas	Linde	UHP
Forming gas (5% H_2 in N_2)	ProSpec	99.99%
Helium gas	Air Products	99.999%

2.2 Methods

2.2.1 Preparation of Nickel Inks

2.2.1.1 Nickel (II) Butyrate MOD Ink Preparation

Fifteen grams of a commercially obtained nickel (II) acetate tetrahydrate was digested in a 60 mL solution of 1-part acetic acid to 1-part acetic anhydride by volume. A Dean-Stark

apparatus using concentrated sulfuric acid was equipped onto the round bottom flask. The solution was then refluxed at 60 °C for 144-168 hours before undergoing vacuum distillation. After refluxing, a conventional vacuum distillation apparatus was fitted onto the boiling flask and the receiving flask was submerged in liquid nitrogen. Volatiles from the just-refluxed solution were then removed under vacuum between 40-60 °C and 10 mTorr until dry, yielding a pale green solid. The solid was then placed into a desiccator for 144-168 hours. After drying in the desiccator, an excess of butyric acid was added to the solid and a Dean-Stark apparatus was equipped onto the flask. The solution was refluxed at 60 °C for another 144-168 hours before undergoing vacuum distillation. After vacuum distillation, the remaining nickel (II) butyrate was vacuum pumped and placed into a desiccator to dry before closing with a ground glass stopper.

A qualitative assessment of the solubility of nickel (II) butyrate (10% w/w) was performed in each of six solvents: pyridine, cyclohexylamine, methacrylic acid, 1-butanol, dimethylethanolamine, and ethanolamine. The pyridine, cyclohexylamine, methacrylic acid, and 1-butanol all resulted in low-viscosity (like water) deep blue liquids, while ethanolamine yielded a viscous (like honey) deep blue liquid. Dimethylethanolamine solutions yielded a viscous teal-blue liquid and were slower to dissolve, needing up to one week of stirring instead of the 1-2 hours that was needed for the other solvents. A concentration of 10% w/w Ni salt in ligand/solvent was arbitrarily chosen for the project.

Film formation from the various nickel (II) butyrate salts listed above was tested. In all but two instances, films were unacceptable due to various reasons including improper wetting of the glass substrates. The two nickel (II) butyrate MOD ink formulations that

yielded acceptable films were in ethanolamine and dimethylethanolamine. These two compositions in were prepared, using the amounts indicated in Table 2 below, under ambient conditions. The solutions were clear and blue, indicating full dissolution of the nickel precursor in the solvents (Figure 1).

Table 2. Preparation of Four Nickel MOD Inks

	Nickel (II) precursor	Amount (g)	Solvent	Amount (g)	Stir time
1	Ni (II) butyrate	0.1014	Ethanolamine	0.9011	1-2 hours
2	Ni (II) butyrate	0.1018	Dimethylethanolamine	0.9065	1 week
3	Ni (II) acetate	0.1001	Ethanolamine	0.9019	1-2 hours
4	Ni (II) acetate	0.1003	Dimethylethanolamine	0.9035	1 week

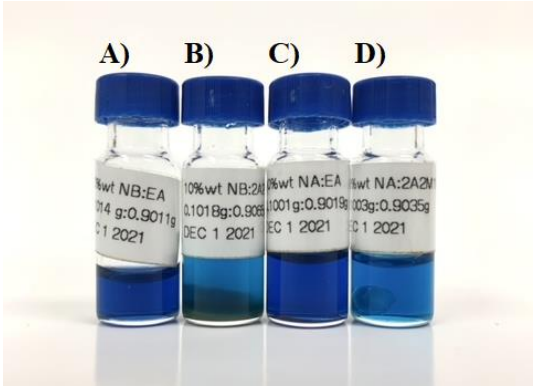

Figure 1. Set of nickel-based MOD ink solutions prepared in December 2021. From left to right. A) 10% w/w nickel (II) butyrate in ethanolamine, B) 10% w/w nickel (II) butyrate in dimethylethanolamine, C) 10% w/w nickel (II) acetate in ethanolamine, D) 10% w/w nickel (II) acetate in dimethylethanolamine.

2.2.1.2 Nickel (II) Acetate MOD Ink Preparation

Two nickel (II) acetate inks were also successfully prepared using the amounts indicated in Table 2. The solutions were clear and blue, indicating full dissolution of the nickel precursor in the solvents (Figure 1). In total, a set of four inks were prepared.

2.2.2 Coating and Film Formation

The Mayer rod deposition method[33-34] (#4 rod, yielding a wet film thickness d~10 µm) was used to cast films of the various nickel-based MOD inks onto uncoated glass microscope slides that were then dried overnight and cured in a tube furnace. The tube furnace was first roughly evacuated, then N_2-purged and specimens were heated (350 ℃ at 5 ℃/min) under flowing forming gas (5% H_2 in N_2, ~0.5 L/min) and then cooled in flowing nitrogen gas (~0.5 L/min) to near room temperature. Other film compositions prepared under identical conditions are shown in Figure 2.

Figure 2. Nickel films made with nickel inks Mayer deposited onto uncoated glass slides and heated to 350 °C in a purged tube furnace under vacuum with flowing forming gas (5% H_2 in N_2, 0.5 L/min). From top to bottom: 10% w/w nickel (II) butyrate in ethanolamine, 10% w/w nickel (II) acetate in ethanolamine, 10% w/w nickel (II) acetate in dimethylethanolamine, 10% w/w nickel (II) butyrate in dimethylethanolamine.

After successfully forming films on uncoated glass slides, the same Mayer rod method was also used to cast films onto Kapton, a polyimide film that is often used in flexible printed

circuits due to its ability to withstand high temperatures, to see if it is possible to successfully form nickel films using this MOD ink solution on this substrate. These films were sintered under the same conditions as the ones formed on the glass substrate and the final films are shown in Figure 3.

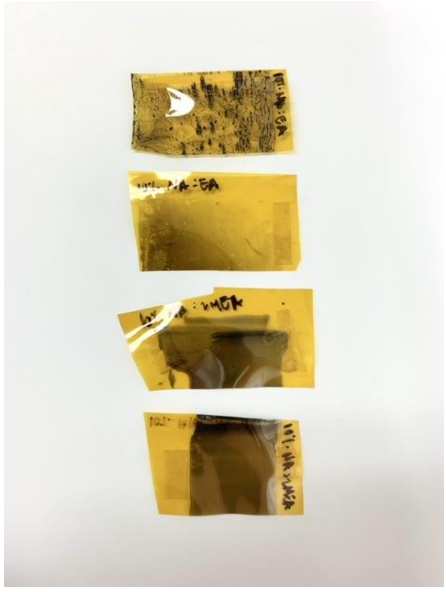

Figure 3. Nickel films made with nickel inks Mayer deposited onto Kapton film and heated to 350 °C in a purged tube furnace under vacuum with 0.5 L/min flowing forming gas (5% H_2 in N_2, 0.5 L/min). From top to bottom: 10% w/w nickel (II) butyrate in ethanolamine, 10% w/w nickel (II) acetate in ethanolamine, 10% w/w nickel (II) butyrate in dimethylethanolamine, 10% w/w nickel (II) acetate in dimethylethanolamine.

3. RESULTS AND DISCUSSION

3.1 Characterization of MOD Inks

The four MOD inks were characterized using Attenuated Total Reflection-Fourier Transform Infrared Spectroscopy (ATR-FTIR), UV-Vis, and X-ray Photoelectron Spectroscopy (XPS) to analyze binding effects, elemental composition, and shelf-stability.

3.1.1 Binding Effects via FTIR

The molecular interaction between each component used to formulate the inks was evaluated by ATR-FTIR, using a Thermoscientific Nicolet iS5. The scans were performed from 500 to 4000 cm^{-1} using a 4 cm^{-1} resolution and an average of 32 scans. As seen in Figures 4-7, FTIR spectra of the solvent and the nickel precursor are compared to the FTIR spectrum of the ink made using the two components. Peaks attributable to features of the molecules under study are indicated in the figures. FTIR spectra are thus consistent with expectation for the starting materials. To discern peaks influenced by complexation of solvent by nickel centers, the data were further analyzed using the LINEST function of Microsoft Excel. This analysis shows relatively small deviations that indicate that the FTIR spectra of the mixtures (prepared inks) were not simply linear sums of the FTIR spectra of the pure components of the mixtures. In this case, LINEST provided a set of two coefficients which when multiplied by the components, sum to a spectrum most like the experimentally measured spectrum of the mixture. Therefore, subtraction of the model spectrum (prepared from the components) from the mixture spectrum yields a residual spectrum. This spectrum may indicate where peaks disappear from the mixture or appear in it. This behavior is

expected as some bonds change characteristics (or are lost) in the components, and some new bonds appear or shift when the solvent binds to the solute. Residual plots for each of the four inks are shown in Figure 8.

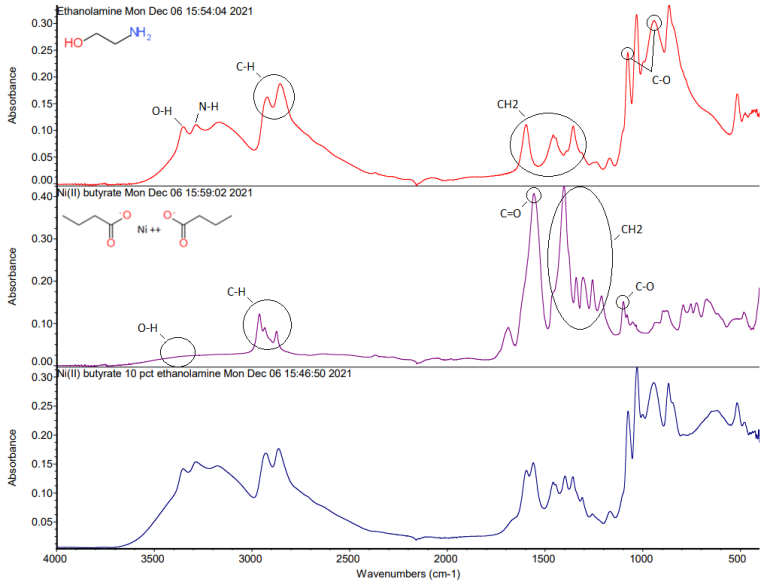

Figure 4. FTIR spectra of ethanolamine (top), nickel (II) butyrate (middle), and 10% w/w nickel (II) butyrate in ethanolamine (bottom).

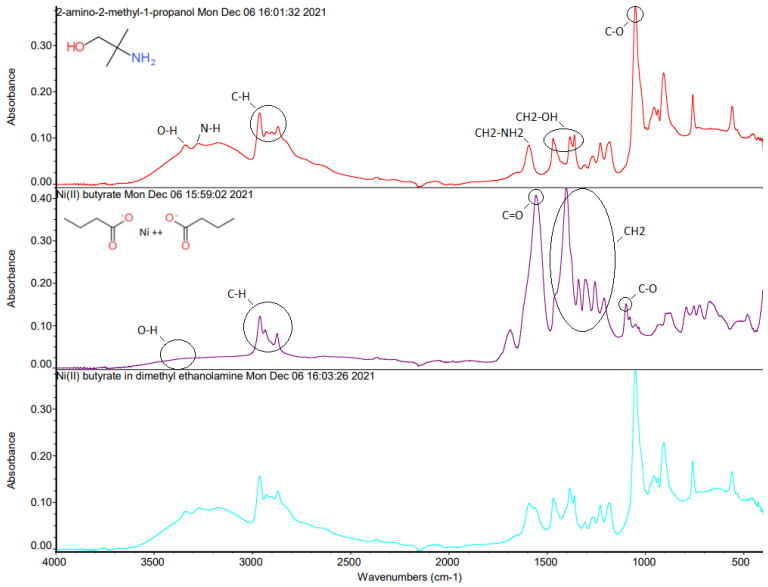

Figure 5. FTIR spectra of dimethylethanolamine (top), nickel (II) butyrate (middle), and 10% w/w nickel (II) butyrate in dimethylethanolamine (bottom).

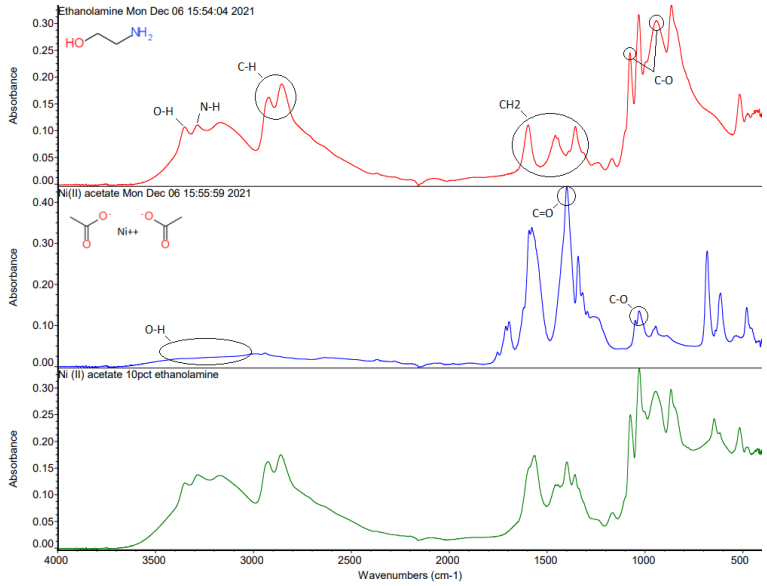

Figure 6. FTIR spectra of ethanolamine (top), nickel (II) acetate (middle), and 10% w/w nickel (II) acetate in ethanolamine (bottom).

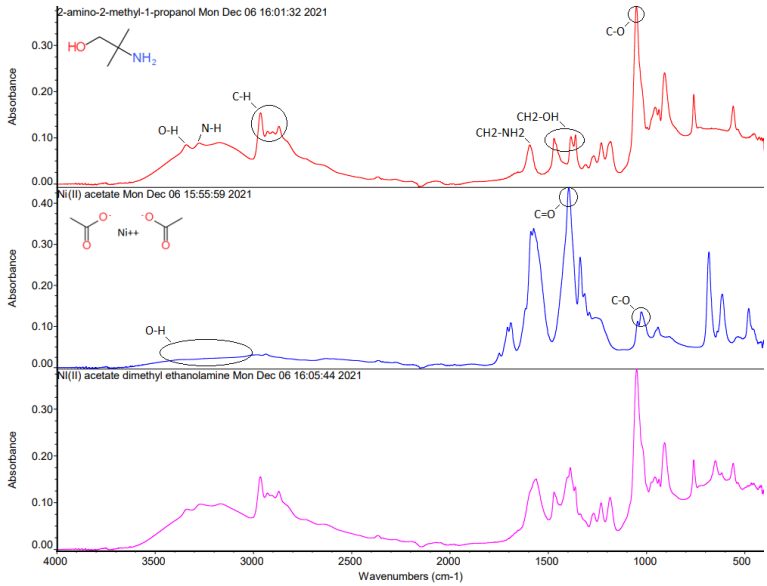

Figure 7. FTIR spectra of dimethylethanolamine (top), nickel (II) acetate (middle), and 10% w/w nickel (II) acetate in dimethylethanolamine (bottom).

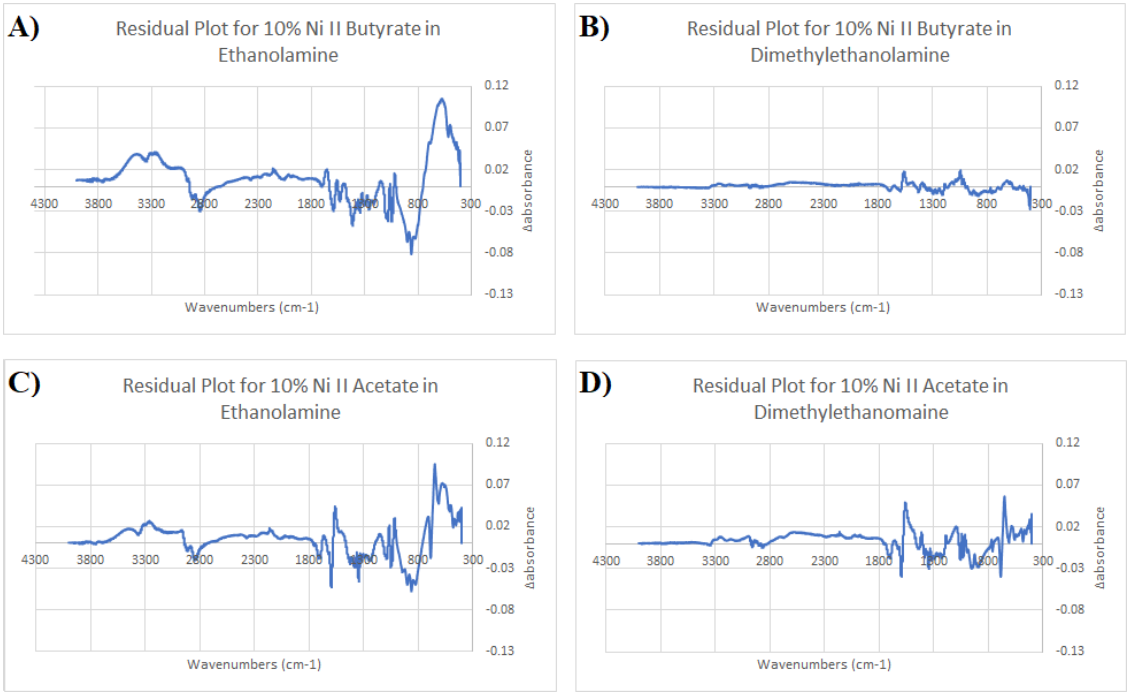

Figure 8. Calculated residual plots to determine binding effects between A) nickel (II) butyrate and ethanolamine, B) nickel (II) butyrate and dimethylethanolamine, C) nickel (II) acetate and ethanolamine, and D) nickel (II) acetate and dimethylethanolamine.

Figures 4 and 5 for nickel (II) butyrate in ethanolamine and nickel (II) butyrate in dimethylethanolamine, respectively, show vibrational modes primarily for O-H around 3400 cm^{-1}, N-H_2 around 3300 cm^{-1}, C-H stretching around 2800-3000 cm^{-1}, C-H_2 rocking around 1500 cm^{-1}, C=O stretching around 1600 cm^{-1} and C-O stretching around 1100 cm^{-1}.

Figures 6 and 7 for nickel (II) acetate in ethanolamine and nickel (II) acetate in dimethylethanolamine, respectively, show vibrational modes primarily for O-H around 3300 cm^{-1}, N-H_2 around 3000 cm^{-1}, C-H stretching around 2900 cm^{-1}, C-H_2 rocking around 1500 cm^{-1}, C=O stretching around 1600 cm^{-1}, and C-O stretching around 1100 cm^{-1}.

Residual plots were constructed by first constructing a model sum from the spectra of the two unperturbed components and then finding the difference between the model sum and the

observed spectrum of the prepared ink, as detailed above. LINEST results of metal salt and solvent are shown in Table 3.

Table 3. ATR-FTIR LINEST Results for the Modeling of Experimental MOD Ink With Experimental Metal Salt and Solvent Spectra

		% Metal Salt	% Solvent
Ni(II) Butyrate	Ethanolamine	25.9 ± 0.4	98.9 ± 0.4
	Dimethylethanolamine	10.3 ± 0.1	93.7 ± 0.1
Ni(II) Acetate	Ethanolamine	28.9 ± 0.3	98.1 ± 0.2
	Dimethylethanolamine	24.4 ± 0.2	97.0 ± 0.2

The LINEST data represents how much of each neat component appears in the spectrum of the mixed ink composition. In theory, the vibrational spectrum of the mixture should differ from that of the components in as much as new bonds appear between, for example, ethanolamine and the nickel center. As can be seen in Table 3, most values sum to > 100%. This may be assigned to changes in the oscillator strength of the various modes, or, more likely to the relatively poor optical contact between the solid metal salt with the planar diamond element in ATR accessory relative to the excellent contact compared to the solvent. Nonetheless, we wish to make the comparison as we feel that it is illustrative in understanding the solvation of the metal centers by ethanolamine and the analogue, dimethylethanolamine.

Major changes in the C-O binding region (~800-1100 cm^{-1}) were observed for inks prepared using ethanolamine (Figures 8a and 8c) but not in the inks prepared using dimethylethanolamine (Figures 8b and 8d). Major changes can also be observed in the O-H and N-H_2 binding regions (~3300-3500 cm^{-1}) in the ethanolamine-based inks as well, and again not in the dimethylethanolamine-based inks. Similar changes can be seen in the C-H_2

rocking frequencies (~1700 cm^{-1}) between the ethanolamine-based and dimethylethanolamine-based inks. It can therefore be inferred that: 1) not surprisingly the ethanolamine solvent likely binds to the metal carboxylates through either the NH or the OH group, and 2) that the ethanolamine-based inks experience a significantly stronger binding affinity to the nickel precursors in each ink.

3.1.2 Binding Stability via UV-Vis

A UV-Vis kinetic study was performed using an Agilent Cary 60 UV-Vis spectrophotometer on each of the four inks, as shown in Figure 9. The scans were performed from 300 to 800 nm with a 1 nm resolution. The binding strength seems to be indifferent with respect to whether a nickel (II) acetate or nickel (II) butyrate was used, but there is a significant shift in wavelength between the spectra seen for the set of ethanolamine-based inks versus the dimethylethanolamine-based inks. The study also supports the conclusion from the FTIR that ethanolamine appears to be a stronger ligand and expands on that conclusion by demonstrating that ethanolamine also seems to more strongly stabilize the nickel (II) complex compared to the dimethylethanolamine. This is indicated by the blue shift of the peaks for ethanolamine, meaning that the Δ energy value in the d-orbital splitting for the ethanolamine ligand in the metal complex is higher. Ethanolamine has a higher field strength than dimethylethanolamine. This difference in the Δ value also contributes to the slight shift in color for the MOD ink liquids seen in Figure 1 (see Methods section). As the difference seems to be relatively small between the ligands, the color shift is also small.

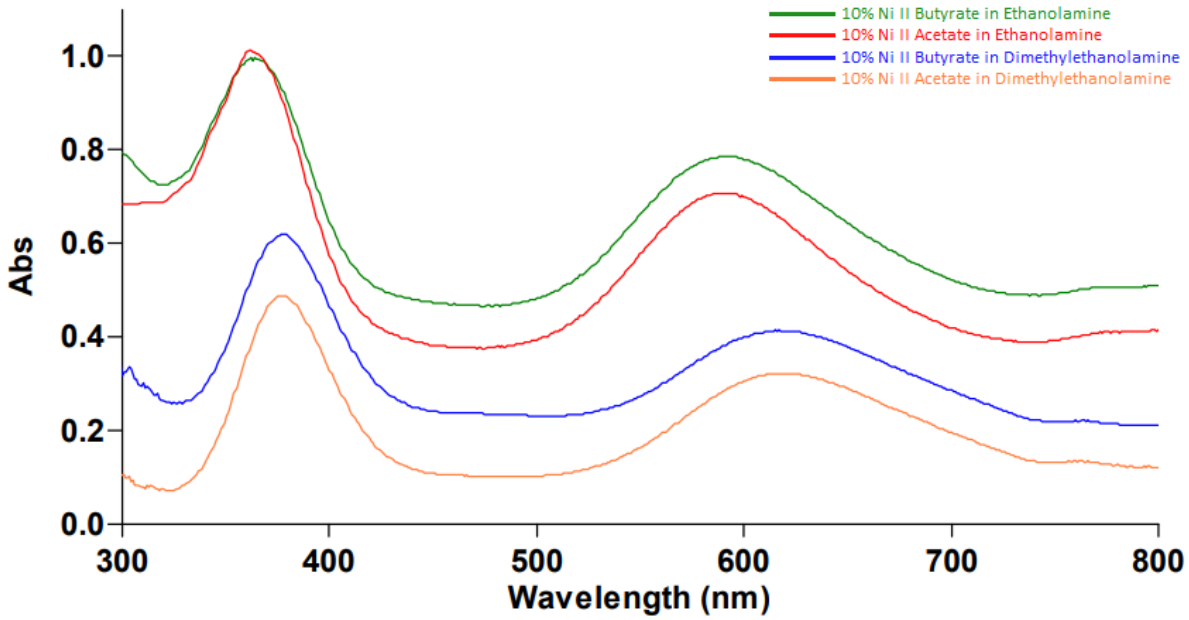

Figure 9. UV-Vis spectra of 10% w/w nickel (II) butyrate in ethanolamine (green), 10% w/w nickel (II) acetate in ethanolamine (red), 10% w/w nickel (II) butyrate in dimethylethanolamine (blue), and 10% w/w nickel (II) acetate in dimethylethanolamine (orange). Spectra were stacked for clarity but are not scaled in intensity.

3.1.3 Chemical Composition via XPS

The chemical composition of the inks was analyzed by producing uncured films dried under vacuum of each ink on uncoated glass slides and performing XPS surface analysis. These data were taken for a 10% w/w nickel (II) butyrate in ethanolamine ink produced in June 2021.

A survey spectrum can be seen in Figure 10. This is a general scan to view the overall elemental composition of the ink. We can also see the same data tabulated in Table 4 below. If there was no contamination in the ink preparation or uncured film casting and drying, only carbon, nitrogen, nickel, and oxygen would be expected in the elemental composition breakdown. However, additional elements sodium, silicon, and sulfur also appear in the

breakdown shown in Table 4. The sodium and silicon may be from the glass slide if the uncured film was particularly thin in the area of analysis and the XPS etched deeper into the glass past the ink layer. Sulfur was not an anticipated contaminant, and the source of this contaminant is unknown.

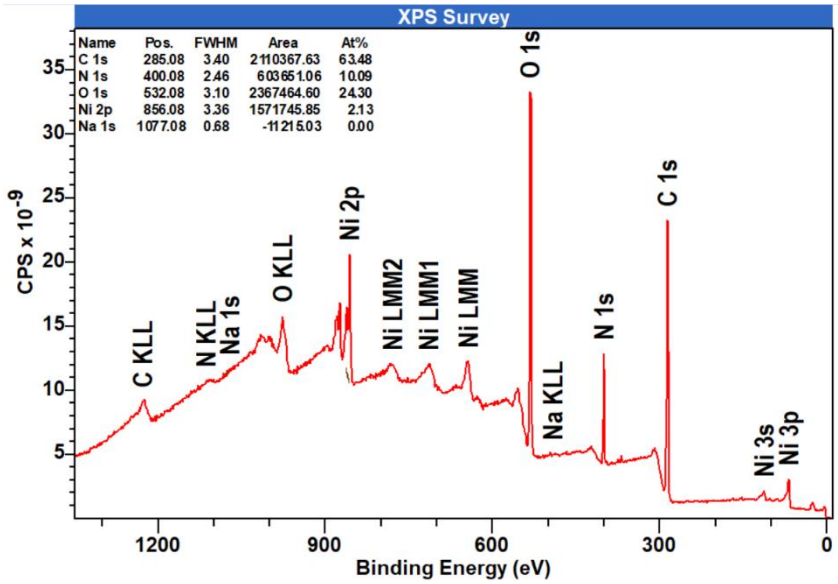

Figure 10. Survey spectrum of the June 2021 10% w/w nickel II butyrate in ethanolamine uncured film with identified peaks.

Table 4. XPS Elemental Breakdown of the June 2021 10% w/w Nickel (II) Butyrate in Ethanolamine Uncured Film on Glass Slide.

Sample	Element	%Atomic Composition
Uncured Film June 2021 10% w/w Nickel (II) butyrate in ethanolamine	C 1s	35.06
	N 1s	16.51
	Na 1s	0.16
	Ni 2p3	3.84
	O 1s	43.86
	S 2p	0.21
	Si 2p	0.35

A high-resolution elemental spectrum for nickel can be seen in Figure 11. The spectrum was further analyzed to determine the species that nickel exists as in the ink. Nickel is

present as nickel hydroxide and nickel oxide in the uncured film, as expected. There are no free nickel ions present in the uncured ink, as it should be bound to the ligand at this stage. There also appears to be much more nickel hydroxide than there is nickel oxide, as shown by the relative peak intensity and percent composition of each component.

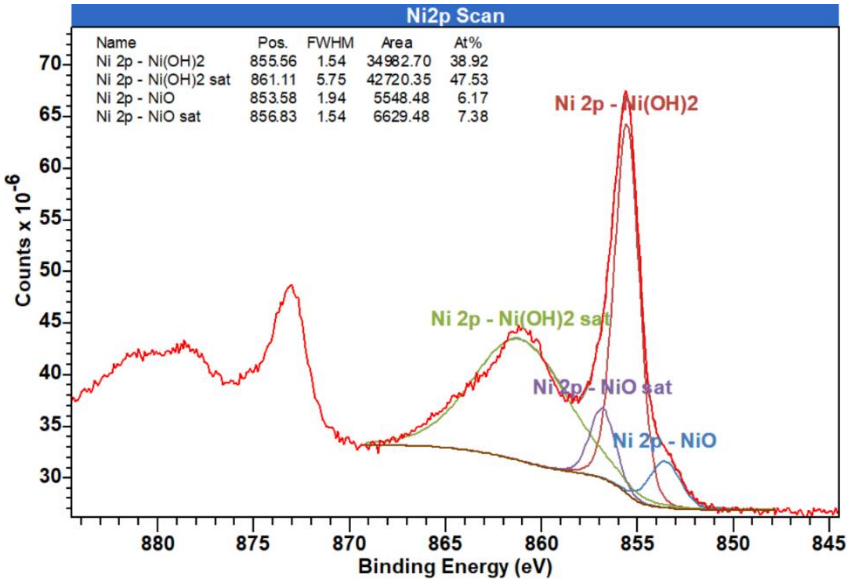

Figure 11. High-resolution nickel elemental spectrum of the June 2021 10% w/w nickel (II) butyrate in ethanolamine uncured film.

3.1.4 Shelf Stability via XPS

The elemental breakdown of two 10% w/w nickel (II) butyrate in ethanolamine inks – one made in June 2021, and one made in September 2021 – were compared to see if there would be any chemical changes in the ink over time. At the time of analysis, the June 2021 (older) ink had been sitting in solution for about four months, while the September 2021 (newer) ink was made a couple days prior to analysis. Table 5 below shows the elemental composition breakdown of the September 2021 ink, and Table 4 above has the breakdown for the June 2021 ink. Looking at the carbon, nitrogen, nickel, and oxygen data between the

two inks, there seem to be negligible differences between the atomic compositions for each element. The most notable changes are shown in the %C 1s, with 35.06% in the June 2021 ink and 38.66% in the Sept 2021 ink, and %N 1s, with 16.51% in the June 2021 ink and 11.27% in the Sept 2021 ink. There is not a prevalent difference in the shelf-stability of ink over time.

Table 5. XPS Elemental Breakdown of the September 2021 10% w/w Nickel (II) Butyrate in Ethanolamine Uncured Film on Glass Slide

Sample	Element	%Atomic Composition
Uncured Film Sept 2021 10% w/w Nickel (II) butyrate in ethanolamine	C 1s	38.66
	N 1s	11.27
	Na 1s	0.78
	Ni 2p3	3.94
	O 1s	43.71
	S 2p	0.92
	Si 2p	0.73

3.2 Characterization of Film Formation

The self-reduction process of nickel-based MOD inks, i.e. the film formation process was characterized by DSC and TGA. These methods ideally give us a step-wise understanding of the thermal decomposition as a whole, either by exo- or endo-thermicity of the events, or by the loss of mass associated with thermally driven processes.

3.2.1 TGA and DSC Profiles

The DSC was done using a TAInstruments DSC 2910 with nitrogen as the carrier gas. Thirty µL of ink was added into the sample pan, equilibrating at 50 ℃ before ramping to 350 ℃ at 5 ℃/min and then cooling from 350 ℃ to 50 ℃ at 5 ℃/min. This was done once per ink to get a total of four DSC thermograms (Figures 12 and 13). The TGA was done using a

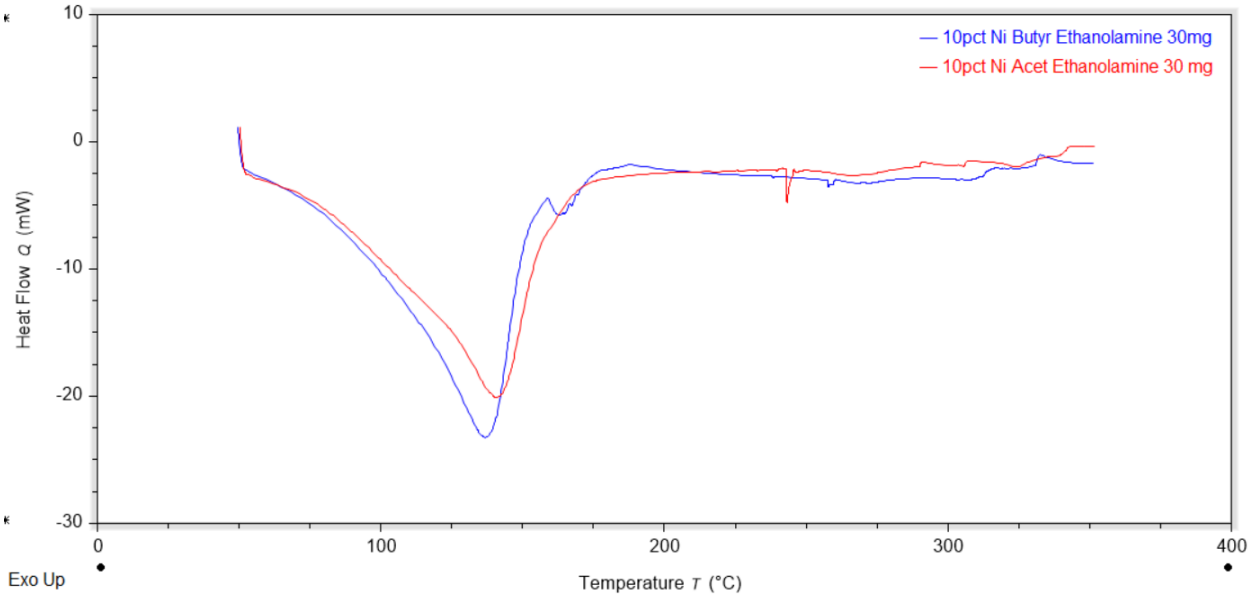

Figure 12. DSC thermogram of 10% w/w nickel (II) butyrate in ethanolamine ink and 10% w/w nickel (II) acetate in ethanolamine ink heated to 350 °C at 5 °C/min under nitrogen conditions.

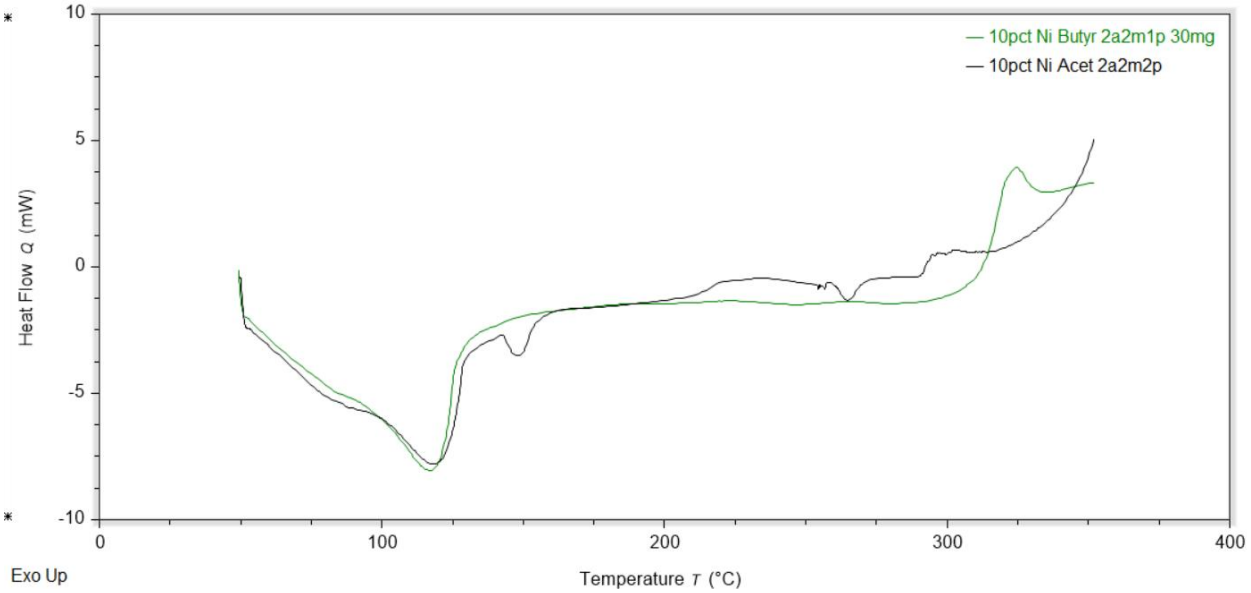

Figure 13. DSC thermogram of 10% w/w nickel (II) butyrate in dimethylethanolamine ink and 10% w/w nickel (II) acetate in dimethylethanolamine ink heated to 350 °C at 5 °C/min under nitrogen conditions.

PerkinElmer TGA 8000 with helium as the carrier gas. Twenty µL of ink was added into each ceramic crucible before loading. The sample was then held for 1 min at 50 ℃ before heating to 400 ℃ at 5 ℃/min and then cooled from 400 ℃ to 50 ℃ at 5 ℃/min. This was done once per ink to get a total of four TGA thermograms (Figures 14-17). The temperatures at which different thermal events occurred are tabulated in Table 6 for comparison.

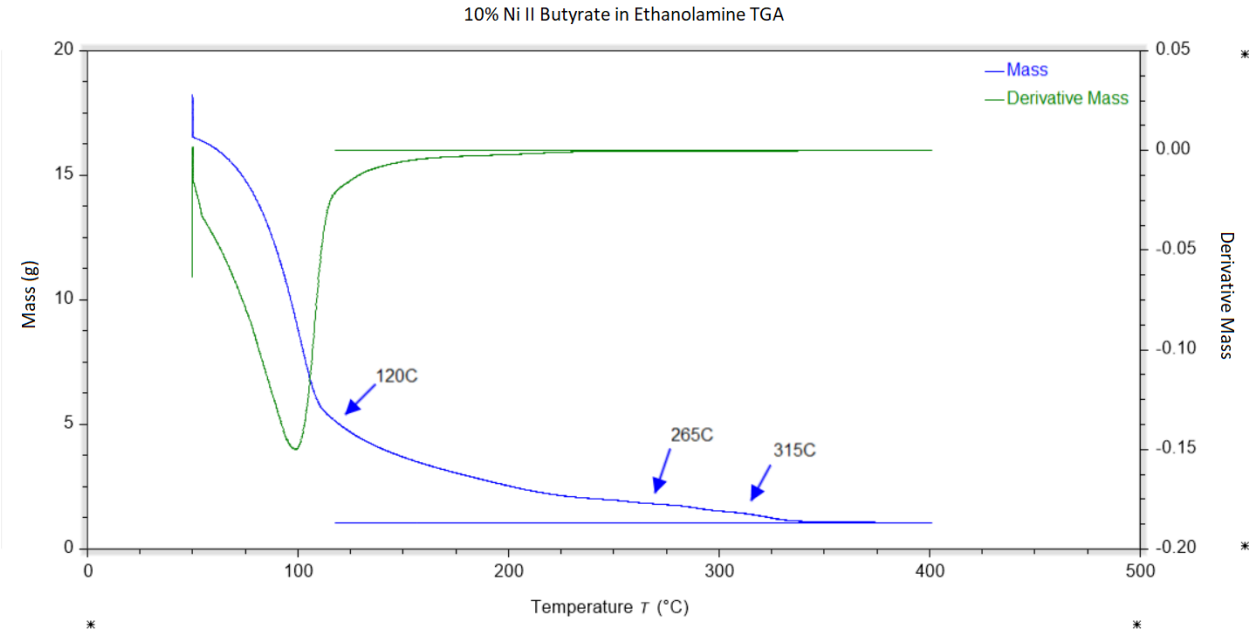

Figure 14. TGA thermogram of 10% w/w nickel (II) butyrate in ethanolamine ink heated to 400 °C at 5 °C/min under helium conditions, including the derivative with respect to temperature.

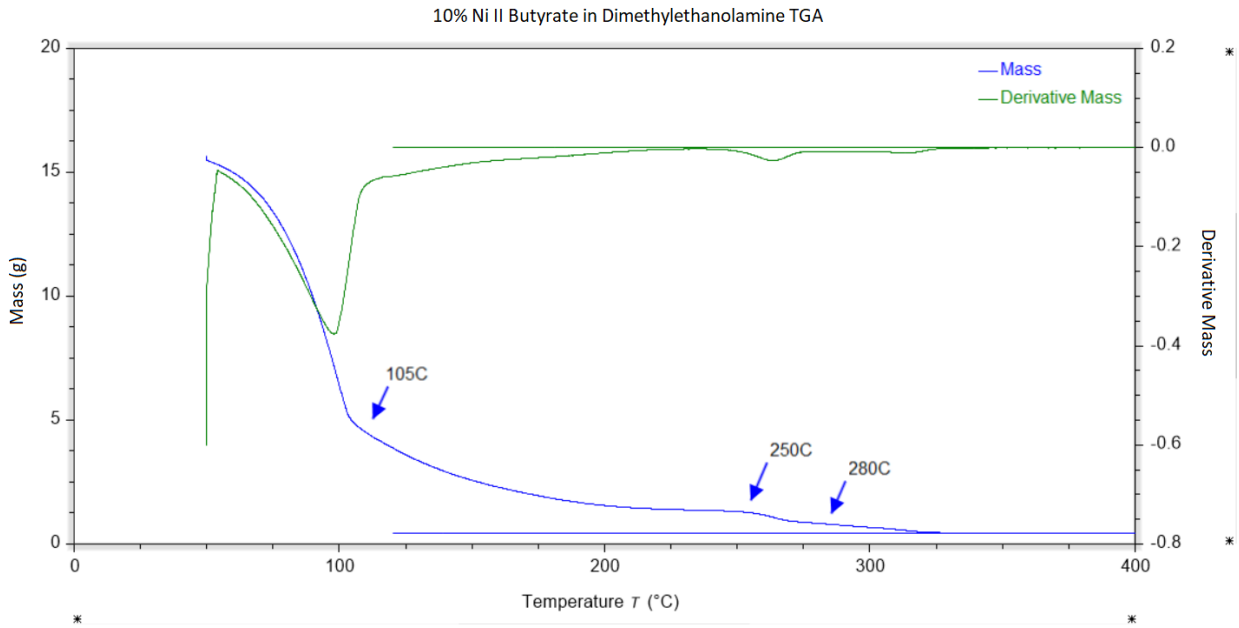

Figure 15. TGA thermogram of 10% w/w nickel (II) butyrate in dimethylethanolamine ink heated to 400 °C at 5 °C/min under helium conditions, including the derivative with respect to temperature.

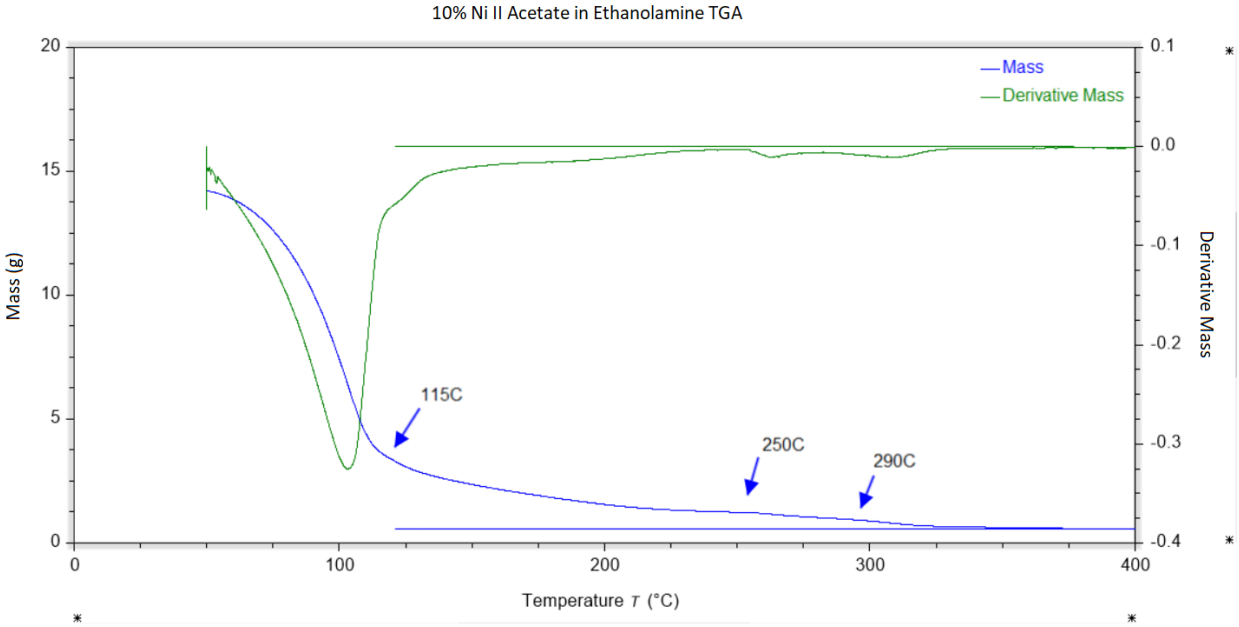

Figure 16. TGA thermogram of 10% w/w nickel (II) acetate in ethanolamine ink heated to 400 °C at 5 °C/min under helium conditions, including the derivative with respect to temperature.

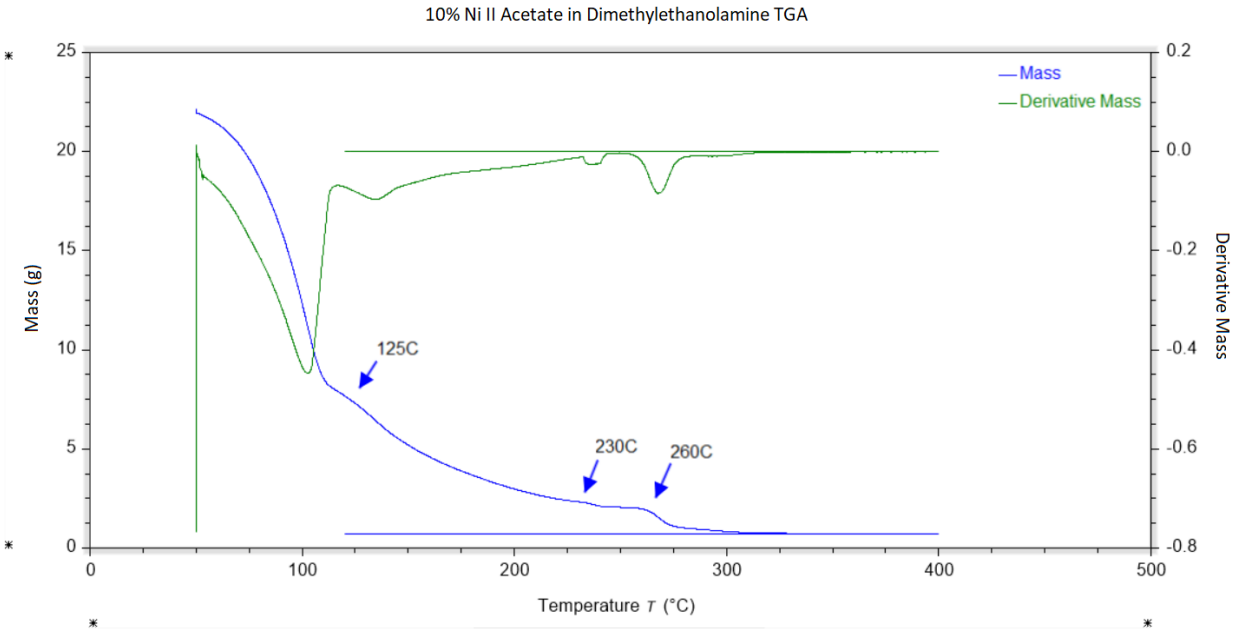

Figure 17. TGA thermogram of 10% w/w nickel (II) acetate in dimethylethanolamine ink heated to 400 °C at 5 °C/min under helium conditions, including the derivative with respect to temperature.

Table 6. Combined TGA-DSC Data to Compare Peaks and the Temperature Where They Occur in Each Respective Thermogram

Ink ID	Peak #	TGA Temp (°C)	DSC Peak Notes	DSC Temp (°C)
10% w/w Ni (II) butyrate in ethanolamine (DSC Fig 12, TGA Fig 14)	1	120	B	160
	2	265	S	260
	3	315	-	-
10% w/w Ni (II) butyrate in dimethylethanolamine (DSC Fig 13, TGA Fig 15)	1	105	B	250
	2	250	-	-
	3	280	-	-
10% w/w Ni (II) acetate in ethanolamine (DSC Fig 12, TGA Fig 16)	1	115	S	240
	2	250	-	-
	3	290	-	-
10% w/w Ni (II) acetate in dimethylethanolamine (DSC Fig 13, TGA Fig 17)	1	125	B	150
	2	230	B	215
	3	260	B	375
	All DSC peaks were endothermic. S = sharp, B = broad (DSC only) Peaks for each TGA and DSC do not necessarily correlate to peaks with the same number in each thermogram.			

From the DSC thermograms, the process seems to be endothermic, with the first peak most likely attributed to ethanolamine or dimethylethanolamine volatilization; around 140 ℃ for ethanolamine in Figure 12 and around 115 ℃ for dimethylethanolamine in Figure 13. The smaller peaks at 160 ℃ and 260 ℃ for nickel (II) butyrate in ethanolamine, 250 ℃ for nickel (II) acetate in ethanolamine, 240 ℃ for nickel (II) butyrate in dimethylethanolamine, and 150 ℃, 215 ℃, and 375 ℃ for nickel (II) acetate in dimethylethanolamine (summarized in Table 6 above) could possibly be nickel decomposition events (from $Ni^{2+} \rightarrow Ni^{0}$).

The TGA thermograms show solvent loss occurring for each ink at around 100 ℃, with subsequent smaller peaks occurring at temperatures indicated in Table 6. The smaller peaks can possibly be attributed to nickel decomposition events (from $Ni^{2+} \rightarrow Ni^{0}$).

Table 6 allows easier comparison between all the inks and their TGA and DSC data. Notes about whether the peak was broad or sharp is indicated by an S for sharp or B for broad in the column to the left of each temperature column. Each peak and the temperatures at which they occur were taken from the thermograms presented in Figures 12-17. In comparing the ethanolamine-based inks and the dimethylethanolamine-based inks, regardless of the nickel complex, it seems that the ethanolamine-based inks require higher temperatures to observe a peak. This correlates strongly with the evidence that ethanolamine is the stronger ligand, as found in the FTIR and UV-Vis data presented earlier in this paper. This is true for both the TGA and DSC data. Ethanolamine stabilizes the ink solutions more than dimethylethanolamine does, requiring higher temperatures to sinter and decompose nickel into film.

As noted above (Methods section) dimethylethanolamine solutions tended to take a longer period of time to dissolve in comparison to the ethanolamine solutions. This is supported by FTIR data (i.e. dimethylethanolamine does not report solvation in the FTIR), and implied by UV-VIS (ethanolamine yielding slightly higher Δ energies for ligand-field stabilization). Interestingly, dimethylethanolamine inks yielded better films, with uniform, smooth mirror surfaces, whereas ethanolamine inks were prone to droplets and pooling, as seen in Figures 2 and 3. We conclude that ethanolamine is bound more strongly and therefore comes off more gradually whereas dimethylethanolamine, more weakly bound, desorbs completely by 260 °C. The last endotherm on each TGA thermogram appears to be the decarboxylation and reduction of $Ni^{2+} \rightarrow Ni^{0}$. DSC are not inconsistent with the above conclusions but have not been reproduced.

3.3 Characterization of the Nickel Films

Characterization of the resulting nickel films were done using XPS and some conductivity measurements.

3.3.1 Analysis of Forming Environment Effects via XPS

A 10% w/w nickel (II) butyrate in ethanolamine ink made in June 2021 was Mayer rod deposited onto cut uncoated glass slides and sintered in a purged tube furnace heated to 300 ℃ at 10 ℃/min and immediately cooled to 60 ℃ before removal. One film was made under a nitrogen gas environment (~0.5 L/min) while a second film was made under a forming gas environment (~0.5 L/min). This was done to see if the gas environment under which the

nickel films were formed would influence the elemental composition of the finished films. To investigate this, XPS analysis was performed on each film.

Figures 18 and 19 show the survey spectra and high-resolution nickel elemental spectrum, respectively, for the 10% w/w nickel (II) butyrate in ethanolamine film made under a nitrogen gas environment. In the high-resolution spectrum, it is shown that the resulting metal film formed under the nitrogen environment does not seem to have any pure nickel in it. Instead, nickel is seen as nickel hydroxide and nickel oxide species in the metal film.

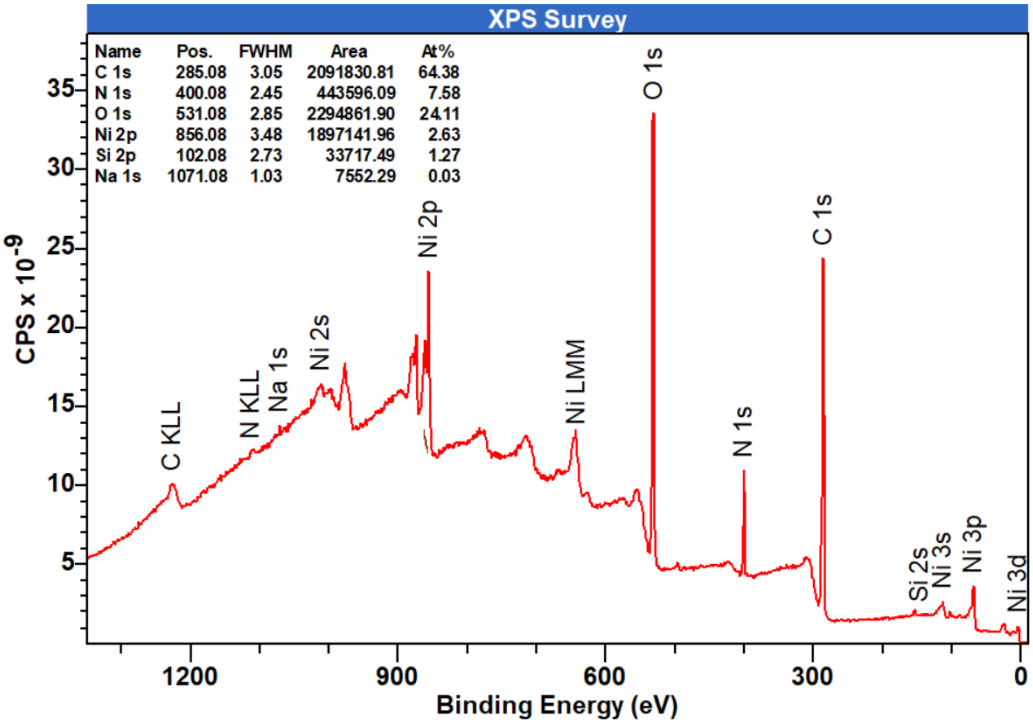

Figure 18. Survey spectrum of the 10% w/w nickel (II) butyrate in ethanolamine metal film formed under nitrogen conditions with identified peaks.

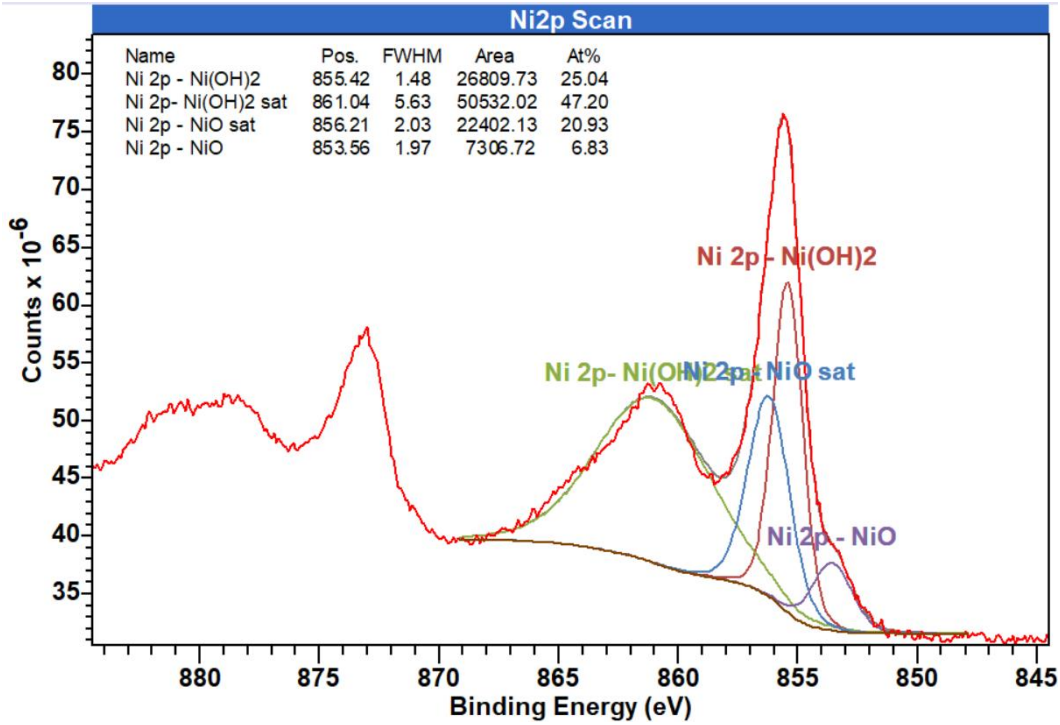

Figure 19. High-resolution nickel elemental spectrum of the 10% w/w nickel (II) butyrate in ethanolamine metal film formed under nitrogen conditions.

Figures 20 and 21 show the survey spectra and high-resolution nickel elemental spectrum, respectively, for the 10% w/w nickel (II) butyrate in ethanolamine film made under a forming gas environment. In the high-resolution spectrum, it is shown that the resulting metal film formed under the forming gas environment also does not seem to have any pure nickel in it, appearing as nickel hydroxide and nickel oxide species instead.

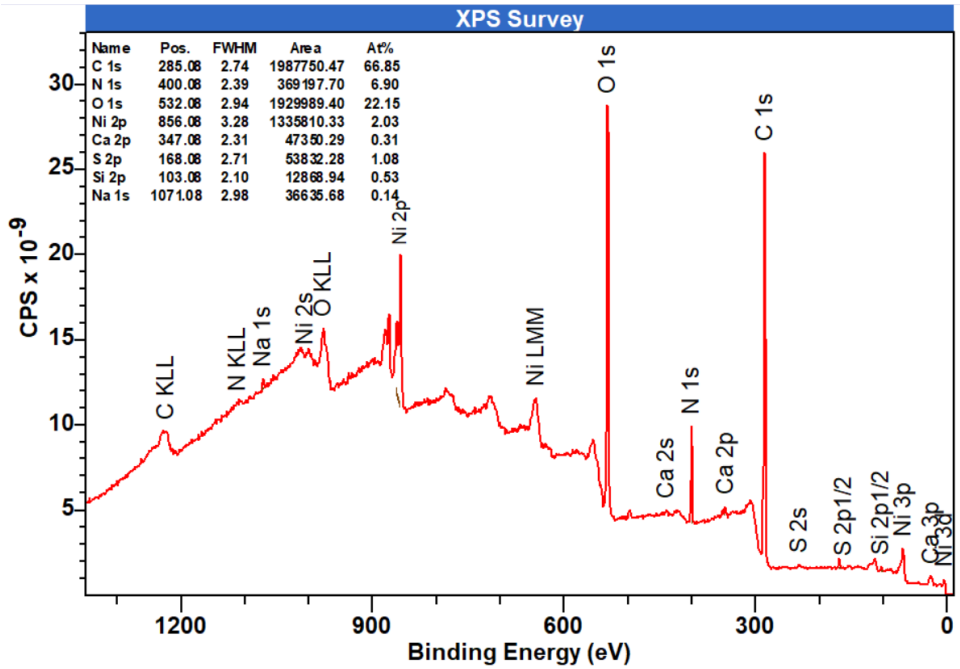

Figure 20. Survey spectrum of the 10% nickel (II) butyrate in ethanolamine metal film formed under forming gas conditions with identified peaks.

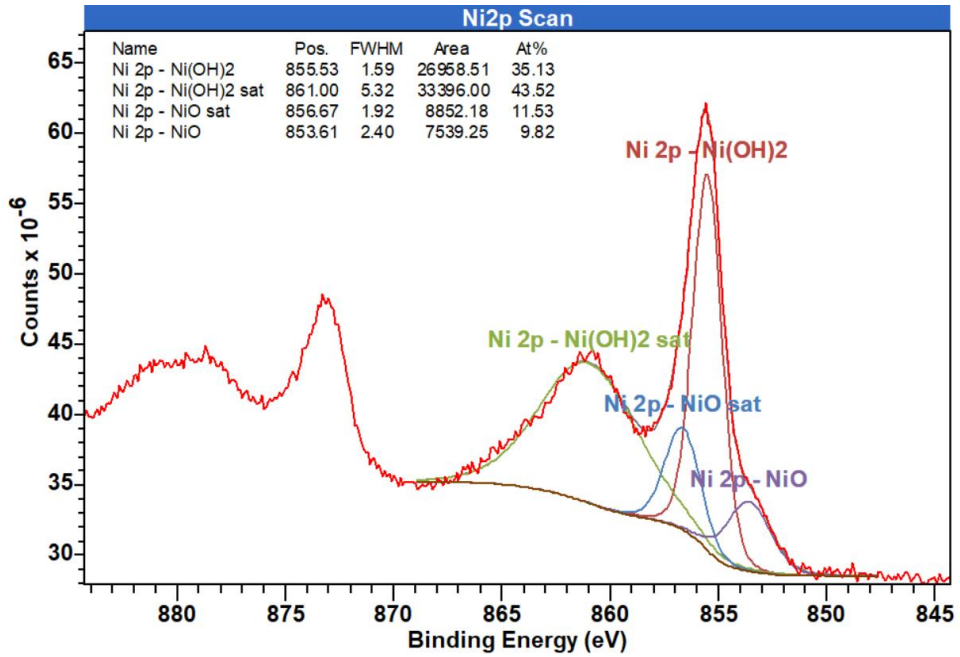

Figure 21. High-resolution nickel elemental spectrum of the 10% nickel (II) butyrate in ethanolamine metal film formed under forming gas conditions.

Comparing the high-resolution spectra seen in Figure 19 and Figure 21, the forming gas environment yields a metal film that has a higher amount of nickel oxide and nickel hydroxide. The metal film formed under nitrogen conditions contains 25.04% nickel hydroxide and 6.83% nickel oxide while the metal film formed under forming gas conditions contains 35.13% nickel hydroxide and 9.82% nickel oxide.

Table 7 shows a quantitative comparison of the atomic composition for each element in the XPS of the uncured film, metal film formed under nitrogen, and metal film formed under forming gas for the June 2021 ink. The gas environment that the ink was sintered in seems to play a significant role in the atomic composition of the final metal films for this formulation. Not only is there significant variation in the amount of each species of nickel present as evident from the high-resolution spectrum, but there is also great variation in the atomic composition of each element found in Table 7 for the metal films formed under different gas environments. The most outstanding difference seen in the %Ni 2p3, where the nitrogen environment yields a metal film with 22.31% Ni 2p3 while the forming gas environment yields a film with 6.99% Ni 2p3. Other significant differences can be seen in %C 1s (10.16% for nitrogen environment, 31.44% for forming gas environment), %N 1s (2.00% for nitrogen environment, 19.76% for forming gas environment, and %O 1s (59.39% for nitrogen environment, 41.82% for forming gas environment).

Table 7. Comparison of XPS Data for the June 2021 10% w/w Nickel (II) Butyrate in Ethanolamine Ink

	Atomic Composition (%)		
Element	Uncured Film	Metal Film (N_2)	Metal Film (H_2/N_2)
C 1s	35.06	10.16	31.44
N 1s	16.51	2.00	19.76
Na 1s	0.16	5.27	0
Ni 2p3	3.84	22.31	6.99
O 1s	43.86	59.39	41.82
S 2p	0.21	0.87	0
Si 2p	0.35	0	0

3.3.2 Analysis of Ink Age Effects on Films via XPS

Shelf stability of the MOD inks was analyzed (see above), and it was found that there was no notable difference in the elemental composition between a freshly prepared ink and the same ink formulation prepared months prior. The effect of MOD ink age on the metal film formed is analyzed here. A metal film was made under nitrogen conditions using a 10% w/w nickel (II) butyrate ink prepared in June 2021 on a cut uncoated glass slide and a second film was made under the same conditions using a 10% w/w nickel (II) butyrate ink made three months later in September 2021. The high resolution nickel XPS spectra for these two films are shown in Figures 22 and 23, respectively.

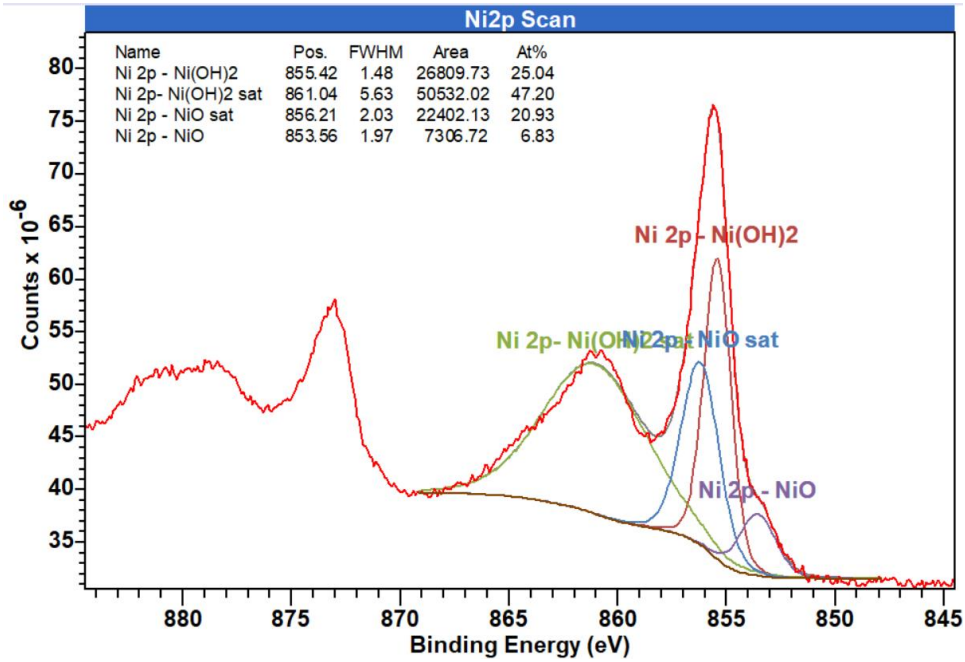

Figure 22. High-resolution nickel elemental spectrum of the metal film formed under nitrogen conditions using 10% nickel (II) butyrate in ethanolamine ink made in June 2021.

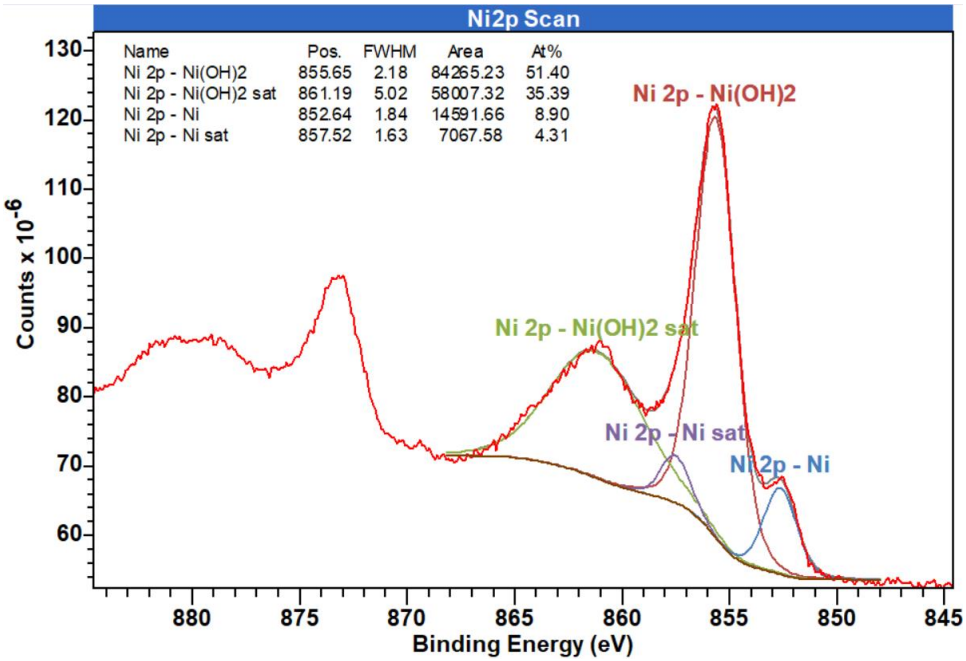

Figure 23. High-resolution nickel elemental spectrum of the metal film formed under nitrogen conditions using 10% nickel (II) butyrate in ethanolamine ink made in Sept 2021.

The most interesting finding is that the film made using the newer September 2021 ink appears to have some metallic nickel in it (8.90%) while the film made using the older June 2021 ink has nickel oxide (6.83%) instead of the metallic nickel. Both films do also contain nickel hydroxide - older ink yielded 25.04% nickel hydroxide while the film made using the newer ink contains 51.40% $Ni(OH)_2$.

3.3.3 Conductivity

Two-probe conductivity measurements were made for the films shown in Figures 2 and 3 (see Methods section), this comprises all of the acetate, butyrate, ethanolamine and dimethylethanolamine Ni(II) MOD inks studied herein. The films were made on uncoated glass microscope slides and showed highly variable wetting behaviors, leaving droplets for the ethanolamine inks but making smooth films for the dimethylethanolamine. The DC conductivity was highly variable and ranged from 24 kW to as low as 60 W for all of the measurements which showed a conductivity value < 200 MW. The films made on Kapton also showed similar magnitude conductivity values.

4. CONCLUSION

Three research goals were explored in this work: ink formulation, film formation, and characterization. We focused on a set of four promising ink formulations that used either ethanolamine or the closely related, but more weakly solvating dimethylethanolamine. The thermal decomposition and films from this decomposition were preliminarily studied by TGA, DSC and then by XPS and conductivity. Our compositions, which were admittedly imperfect in terms of the highly variable conductivity results and their blackened mirror appearances, did show reduced Ni in one case, and thus indicate that this approach may be viable for preparing conductive films with minimal oxide and minimal contamination. Notably these films were successfully fabricated on both glass substrates and flexible Kapton film, strongly hydrophilic and hydrophobic substrates respectively, but yielding similar results.

From the perspective of the MOD ink formulations, ethanolamine was found to be the stronger binding ligand which should more strongly stabilize the Ni complexes. This is supported by the FTIR, UV-Vis, and DSC/TGA data. Also in the case of ethanolamine, O-Ni interactions are most likely occurring. Unfortunately, we do not have XPS data for the dimethylethanolamine to compare the O-Ni compositions. In terms of shelf-stability, it was found that the inks were stable when left as solutions under ambient conditions over a period of a couple months.

The film formation and self-reduction process seems to be endothermic, as demonstrated by the combined DSC/TGA data. There seems to be three main events (as shown by TGA):

solvent volatilization around 120 ℃, desorption of the ligand by 260 ℃, and the decarboxylation and reduction of $Ni^{2+} \rightarrow Ni^0$ in the 280-315 ℃ range.

XPS data indicate that the gas environment (presence of H_2 in N_2) which the films were formed plays a significant role on the final atomic composition of the metal films, at least for the nickel (II) butyrate in ethanolamine formulation, wherein N_2 curing favored a more Ni^0-rich film. The age of the ink at the time of film formation could have a role in whether or not metallic nickel will appear on the metal film surface, as older ink lacked a Ni^0 peak in XPS.

4.1 Future Direction

There are still many unknowns in the film formation chemistry and metal film morphology for nickel films made with MOD inks. In future work, more TGA and DSC replicates are needed to help define the self-reduction process more clearly. TGA-mass spectrometry (TGA-MS) and gas chromatography-mass spectrometry (GC-MS) could also be great tools in determining the gas-phase products produced during thermal decomposition to further characterize the self-reduction process.

Microscopy (i.e., scanning electron microscopy, transmission electron microscopy, atomic force microscopy) can be used to analyze the film surfaces for smoothness/roughness and uniformity. Four-probe conductivity and other electrochemical measurements can also be applied to analyze surface chemistry of the finished metal films. It would also be interesting to see what kind of effects on film morphology using a wider variety of substrates can have.

Currently, the curing temperature of the ink materials explored in this work is higher than desired (< 250℃, for use on flexible substrates like plastics). One way to address this is to determine what changes to the ink formulation could potentially result in lower curing temperatures (from 300-350 ℃ currently to 250 ℃ ideally). Some changes could include exploring metal-alloy based formulations (ex: Ni-Au, Ni-Cu, etc) or exploring mixtures of solvents and other additives. These changes can also improve the coating properties of the nickel ink materials and could potentially address the issue of oxide formation on the finished films as well. Ultimately, the inks should be usable in an inkjet printer type of fabrication device and create conductive, even films.

REFERENCES

1. Mbam, S. O.; Nwonu, S. E.; Orelaja, O. A.; Nwigwe, U. S.; Gou, X.-F., Thin-film Coating; Historical Evolution, Conventional Deposition Technologies, Stress-state Micro/Nano-level Measurement/Models and Prospects Projection: a Critical Review. *Mater. Res. Express* **2019,** *6* (12), 122001.

2. Thakur, N.; Murthy, H., Nickel-Based Inks for Inkjet Printing: A Review on Latest Trends. *Am. J. Mater. Sci.* **2021,** *11*, 20-35.

3. Yang, W.; List-Kratochvil, E. J. W.; Wang, C., Metal Particle-free Inks for Printed Flexible Electronics. *J. Mater. Chem. C* **2019,** *7* (48), 15098-15117.

4. Curtis, C. J.; Rivkin, T.; Miedaner, A.; Alleman, J.; Perkins, J.; Smith, L.; Ginley, D., Metallizations by Direct-Write Inkjet Printing: Preprint. In *Conference Paper:* Proceedings of the 2001 NCPV Program Review Meeting, Lakewood, CO (US), Oct. 14-17, 2001. National Renewable Energy Lab, Golden, CO, 2001.

5. Kamyshny, A.; Steinke, J.; Magdassi, S., Metal-based Inkjet Inks for Printed Electronics. *The Open Appl. Phys. J.* **2011,** *411*, 19-36.

6. Li, J.; Rossignol, F.; Macdonald, J., Inkjet Printing for Biosensor Fabrication: Combining Chemistry and Technology for Advanced Manufacturing. *Lab Chip* **2015,** *15* (12), 2538-2558.

7. DeBruin, D. Formulating a Particle-Free and Low Temperature Nickel Reactive Ink for Inkjet Printing Conductive Features. M.S., Arizona State University: Tempe, AZ, **2019**.

8. Choi, Y.; Seong, K.-d.; Piao, Y., Metal−Organic Decomposition Ink for Printed Electronics. *Adv. Mater. Interfaces* **2019,** *6* (20), 1901002.

9. Kim, S.-H.; Choi, K.-H.; Cho, S.-J.; Choi, S.; Park, S.; Lee, S.-Y., Printable Solid-State Lithium-Ion Batteries: A New Route toward Shape-Conformable Power Sources with Aesthetic Versatility for Flexible Electronics. *Nano Lett.* **2015,** *15* (8), 5168-5177.

10. Kang, D.; Young, J. L.; Lim, H.; Klein, W. E.; Chen, H.; Xi, Y.; Gai, B.; Deutsch, T. G.; Yoon, J., Printed Assemblies of GaAs Photoelectrodes With Decoupled Optical and Reactive Interfaces for Unassisted Solar Water Splitting. *Nat. Energy* **2017,** *2* (5), 17043.

11. Hakola, L.; Parra-Puerto, A.; Vaari, A.; Maaninen, T.; Kucernak, A.; Viik, S.; Smolander, M., Anode Ink Formulation for a Fully Printed Flexible Fuel Cell Stack. *Flexible Printed Electron.* **2020,** *5*.

12. Syukri; Ban, T.; Ohya, Y.; Takahashi, Y., A Simple Synthesis of Metallic Ni and Ni–Co Alloy Fine Powders from a Mixed-metal Acetate Precursor. *Mater. Chem. Phys.* **2003,** *78* (3), 645-649.

13. Park, B. K.; Kim, D.; Jeong, S.; Moon, J.; Kim, J. S., Direct Writing of Copper Conductive Patterns by Ink-jet Printing. *Thin Solid Films* **2007,** *515* (19), 7706-7711.

14. Chang, C.-W.; Cheng, T.-Y.; Liao, Y.-C., Encapsulated Silver Nanoparticles in Water/Oil Emulsion for Conductive Inks. *J. Taiwan Inst. Chem. Eng.* **2018,** *92*, 8-14.

15. R, V. K. R.; K, V. A.; P. S, K.; Singh, S. P., Conductive Silver Inks and their Applications in Printed and Flexible Electronics. *RSC Adv.* **2015,** *5* (95), 77760-77790.

16. Dong, Y.; Lin, Z.; Li, X.; Zhu, Q.; Li, J.-G.; Sun, X., A Low Temperature and Air-sinterable Copper–Diamine Complex-based Metal Organic Decomposition Ink for Printed Electronics. *J. Mater. Chem. C* **2018,** *6* (24), 6406-6415.

17. Schoner, C.; Tuchscherer, A.; Blaudeck, T.; Jahn, S. F.; Baumann, R. R.; Lang, H., Particle-free Gold Metal–Organic Decomposition Ink for Inkjet Printing of Gold Structures. *Thin Solid Films* **2013,** *531*, 147-151.

18. Shin, D.-H.; Woo, S.; Yem, H.; Cha, M.; Cho, S.; Kang, M.; Jeong, S.; Kim, Y.; Kang, K.; Piao, Y., A Self-Reducible and Alcohol-Soluble Copper-Based Metal–Organic Decomposition Ink for Printed Electronics. *ACS Appl. Mater. Interfaces* **2014,** *6* (5), 3312-3319.

19. Szczęsny, R.; Szłyk, E., Thermal Decomposition of Some Silver(I) Carboxylates Under Nitrogen Atmosphere. *J. Therm. Anal. Calorim.* **2013,** *111* (2), 1325-1330.

20. Deng, D.; Qi, T.; Cheng, Y.; Jin, Y.; Xiao, F., Copper Carboxylate With Different Carbon Chain Lengths as Metal–Organic Decomposition Ink. *J. Mater. Sci.: Mater. Electron.* **2014,** *25* (1), 390-397.

21. Pajor-Świerzy, A.; Socha, R.; Pawłowski, R.; Warszyński, P.; Szczepanowicz, K., Application of Metallic Inks Based on Nickel-Silver Core–Shell Nanoparticles for Fabrication of Conductive Films. *Nanotechnol.* **2019,** *30* (22), 225301.

22. Park, S.-H.; Kim, H.-S., Flash Light Sintering of Nickel Nanoparticles for Printed Electronics. *Thin Solid Films* **2014,** *550*, 575-581.

23. Ramachandran, H.; Jahanara, M. M.; Nair, N. M.; Swaminathan, P., Metal Oxide Heterojunctions Using a Printable Nickel Oxide Ink. *RSC Adv.* **2020,** *10* (7), 3951-3959.

24. Pasquarelli, R.; Curtis, C.; Van Hest, M., Inkjet Printing of Nickel and Silver Metal Solar Cell Contacts. *Energy J.* **2007**, 91-96.

25. Li, D.; Sutton, D.; Burgess, A.; Graham, D.; Calvert, P., Conductive Copper and Nickel Lines via Reactive Inkjet Printing. *J. Mater. Chem.* **2009,** *19* (22), 3179-3724.

26. Petukhov, D. I.; Kirikova, M. N.; Bessonov, A. A.; Bailey, M. J. A., Nickel and Copper Conductive Patterns Fabricated by Reactive Inkjet Printing Combined with Electroless Plating. *Mater. Lett.* **2014,** *132*, 302-306.

27. Ginley, D. S.; Curtis, C. J.; Miedaner, A.; van Hest, M. F. A. M.; Kaydanova, T. (12) United States Patent (10) Patent No .: US 8641931 B2, 2014.

28. Wu, Y.; Li, Y.; Liu, P.; Gardner, S.; Ong, B. S., Studies of Gold Nanoparticles as Precursors to Printed Conductive Features for Thin-Film Transistors. *Chem. Mater.* **2006,** *18* (19), 4627-4632.

29. Lai, C. Y.; Cheong, C. F.; Mandeep, J. S.; Abdullah, H. B.; Amin, N.; Lai, K. W., Synthesis and Characterization of Silver Nanoparticles and Silver Inks: Review on the Past and Recent Technology Roadmaps. *J. Mater. Eng. Perform.* **2014,** *23* (10), 3541-3550.

30. Min, H., Preparation and Characterization of Nickel Oxide Thin Films: A review. *Int. J. Appl. Chem.* **2016,** *12*, 87-93.

31. Choi, Y.-H.; Hong, S.-H., Effect of the Amine Concentration on Phase Evolution and Densification in Printed Films Using Cu(II) Complex Ink. *Langmuir* **2015,** *31* (29), 8101-8110.

32. Hayami, Y., The Stabilities of Metal Ammine Complexes. I. The Absorption Spectra of a Series of Hexammine Ni(II) and Tetrammine Pt(II) Complexes. *Bull. Chem. Soc. Jpn.* **1957,** *30* (2), 132-135.

33. Kitano, T.; Maeda, Y.; Akasaka, T., Preparation of Transparent and Conductive Thin Films of Carbon Nanotubes Using a Spreading/Coating Technique. *Carbon* **2009,** *47* (15), 3559-3565.

34. Meng, Y.; Xu, X.-B.; Li, H.; Wang, Y.; Ding, E.-X.; Zhang, Z.-C.; Geng, H.-Z., Optimisation of Carbon Nanotube Ink for Large-area Transparent Conducting Films Fabricated by Controllable Rod-coating Method. *Carbon* **2014,** *70*, 103-110.